

Water adsorption on Pd {100} from first principles

Jibiao Li,^{*,†} Shenglong Zhu, Ying Li, and Fuhui Wang^{*,‡}

State Key Laboratory for Corrosion and Protection (SKLCP), Institute of Metal Research (IMR), Chinese Academy of Sciences (CAS),
62 Wencui Road, Shenyang 110016, China

(Received 1 March 2007; published 27 December 2007)

The adsorption of isolated H₂O on Pd {100} has been investigated by density functional theory calculations. We have presented a detailed picture for the adsorption of water monomer on various high-symmetry sites of the surface. We have demonstrated that other *d* orbitals are responsible for the water adsorptions, in addition to the well-recognized role of *d*_z² orbital. Furthermore, Pd 5 *s* state was found to play an essential role in water adsorptions including the favored on-top case. Our findings augment existing knowledge of the electronic nature of water-metal interactions.

DOI: [10.1103/PhysRevB.76.235433](https://doi.org/10.1103/PhysRevB.76.235433)

PACS number(s): 68.43.Bc

I. INTRODUCTION

Water adsorption on metal surfaces is one of the fundamental topics in surface science and is considered relevant for a better understanding of surface phenomena such as heterogeneous catalysis, corrosion of materials, and surface electrochemistry. Among the considerable efforts,^{1,2} adsorption models of water have attracted widespread interests in the scientific community.^{3,4} From a practical point of view, it is critical to understand whether water adsorbs in the molecular state or dissociates, due essentially to roles of the dissociation products (proton ions and hydroxyl ions) in metal corrosion. For the catalytic surface reaction H₂+O₂→H₂O on palladium, water adsorption is a key factor that further affects reaction kinetics^{5,6} in the same way as water dissociation is in water splitting reactions.⁷ An investigation of H₂O molecules on Pd, therefore, is not only vital to understanding H₂O-Pd interactions and providing a prototype model for understanding metal corrosion at the atomic level, but it also enriches our knowledge of one-molecule chemistry at metal surfaces.

Characterizations of H₂O adsorption on low-index surfaces of palladium have been performed by several groups employing various surface analytical techniques. By using electron energy loss spectroscopy^{8–11} (EELS) and vibrational analysis,¹² the water monomer has been found to adsorb on atop site of Pd {100}, with the molecular plane significantly tilted relative to the substrate at temperature of about 10 K. The existence of monomeric water on Pd{110} (Ref. 13) has been evidenced by techniques of high resolution electron energy loss spectroscopy (HREELS) and temperature programmed desorption (TPD). Brosseau *et al.*^{14,15} further provided detailed information concerning the geometry and bonding of the adsorbed water on Pd {110} with the consideration of coverage effect, supporting adsorption models from water clusters to a bilayer structure. In addition, HREELS measurements combined with TPD have demonstrated that water adsorbs molecularly on Pd {110} at 100 K, and that increasing the temperature to about 200 K gives rise to H₂O desorption from its adsorption site.¹⁶ The same behavior was found for bilayer water on Pd (111) when increasing temperature.^{17,18} By means of work function and mass resolved TPD, Heras *et al.*¹⁹ found that H₂O adsorbs molecu-

larly and binds to the surface through the O atom and that H₂O desorption involves molecule rebuilding at *T*>220 K. The results of low-energy electron diffraction (LEED) have shown that exposure of H₂O to Pd {110} in the range of 100–172 K produces the *c*(2×2) pattern,²⁰ and the *c*(1×1) structure was observed on heating to 213 K. Recent scanning tunneling microscopy investigations by Mitsui *et al.*²¹ revealed that icelike puckered hexagonal units form by successive addition of water monomer on Pd {111}, which is further responsible for water overlayer growth on the surface.²²

Water-metal interactions have been studied theoretically by several earlier *ab initio* studies aimed at providing definite structures as well as energies for water adsorption.^{3,4} The model of flat-lying configurations of on-top adsorption for isolated H₂O is well established, as well as the icelike bilayer structure for H₂O adsorption.^{23,24} As to the nature of the bonding in these models, the following systems have been reported: H₂O/Ru {1000},²⁵ H₂O/Pt {111},^{26,27} H₂O/Ag {111},²⁸ H₂O/Ni,²⁹ and H₂O/Cu {100}.³⁰ Insight into the surface bonding mechanisms which were previously treated as lone-pair interactions³¹ has been provided, whereby the common feature can be considered as interactions of the molecular orbital *b*₁ of H₂O with atomic *d* orbital of bonded metal atoms, resulting in flat-lying configurations for water monomers on the surfaces. Nonetheless, no previous effort focused on offering partial density of states (PDOS) was made to understand the precise nature of water adsorptions. H₂O adsorptions on Pd {100}, a simple and ideal model of this consideration, have not been reported so far. Unlike the close packed surface of Pd {111}, a detailed investigation on the electronic nature of water adsorption on the more open surface is indispensable to a complete understanding of water-metal interactions. In this paper, a careful study on geometrical and electronic structures of H₂O adsorption on Pd {100} is presented through the analysis of electron density difference and projected density of states. Different binding mechanisms for the favored on-top adsorption as well as metastable adsorptions have been presented. In addition to the well-recognized role of *d*_z² orbital, we have shown that some other *d* orbitals as well as Pd 5*s* state play indispensable roles in the adsorption.

TABLE I. Slab thickness (I), cell size (II), k point (III), and cut effect (IV) on adsorption energy of water monomer near atop site. (2×2) unit cell was used for the layer and k -point dependence.

Layer	I	II	E (meV)	III	E (meV)	IV	E (meV)
	E (eV)	Cell (k point)		k point		ecut (Ry)	
5	-0.28	2×2 ($5 \times 5 \times 1$)	-271	$3 \times 3 \times 1$	-276	35	-0.271
7	-0.28			$5 \times 5 \times 1$	-271	38	-0.271
9	-0.28	3×3 ($3 \times 3 \times 1$)	-302	$7 \times 7 \times 1$	-271	40	-0.271

II. COMPUTATIONAL METHODS

All the calculations were performed in the framework of density functional theory approach as implemented by the PWSCF code contained in the QUANTUM ESPRESSO package.³² All the molecular graphics were produced by the XCRYSDEN software package.³³ Electron-ion interactions were included through the use of ultrasoft pseudopotentials.³⁴ Electron exchange and correlation effects were described by the generalized gradient approximation of Perdew *et al.*^{35,36} for accuracy in dealing with the water-metal interactions. Kohn-Sham orbitals were expanded in a plane wave basis set with a cutoff energy of 38 Ry (300 Ry for the charge density cutoff). A Monkhorst-Pack mesh³⁷ within the surface Brillouin zone was used. Brillouin zone integration was performed by the Gaussian-smearing special point technique, with a smearing parameter of 0.05 Ry.

The clean Pd $\{100\}$ surface was modeled by an extended system of a five-layer slab separated by a vacuum region of 12 Å. Water was placed on both sides of the slab of a unit cell of 2×2 size to simulate the adsorbed system. The k -point samplings of $3 \times 3 \times 1$ and $5 \times 5 \times 1$ were employed in the present calculations. Structure optimizations were performed with the slab atoms fixed at their bulk-determined positions, and the adsorbed water was fully relaxed until the Hellmann-Feynman forces were lower than 0.001 Ry/a.u. A calculation was considered converged when the energy per atom was less than 1×10^{-5} Ry and the mean displacement of the atoms was less than 0.001 Å.

Convergence tests of the total energy with respect to cutoff energies (up to 78 Ry) and k points were performed on a bare slab as well as a cubic cell representing the bulk Pd. The absolute total energy was found to converge to 5 meV/atom at 38 Ry, and the energy differences were within only 8 meV/atom for various k -point samplings (from $3 \times 3 \times 1$ to $12 \times 12 \times 1$). Although our test calculations exhibit certain cell-size effect on the adsorption energy, the supercell used here is large enough to avoid interactions between H₂O molecules, as indicated in previous investigations of monomeric water on other metal surfaces.^{26,30} The convergence of the adsorption energy of H₂O was checked using the cutoff energy up to 42 Ry. For the sake of accuracy and validity of our results, variations of the adsorption energy with respect to layer thickness, cell size, cutoff energy and k -point sampling are presented in Table I.

The rest of the paper is organized as follows. We initially studied the properties of the bulk Pd and the bare Pd $\{100\}$

surface as well as water molecules of gas phase, followed by equilibrium properties including adsorption geometry and binding energy of the stable and metastable configurations of H₂O. The results concerning the bonding nature are given in the Sec. III, followed by the conclusions in Sec. IV.

III. RESULTS AND DISCUSSIONS

A. Bulk and surface properties

The structure and energy of the isolated gas phase water were calculated within a box with the same sizes of the absorbed systems. The optimized geometry for free H₂O gives a bond length of 0.97 Å and a bond angle of 104.5°, which are in line with the experimental values³⁸ of 0.96 Å and 104.5°, respectively. Calculations for bulk Pd were performed with a cutoff energy of 38 Ry and a k mesh of $12 \times 12 \times 12$, in which total energy was converged within 5 meV per atom, varying cutoff energy up to 78 Ry. The obtained lattice constant (3.97 Å) for palladium is also in good agreement with the experimental value (3.89 Å). For relaxation of clean Pd $\{100\}$ (Table II), we show that the first Pd interlayer spacing (d_{12}) exhibits an inward relaxation, and

TABLE II. Interlayer relaxation of Pd $\{100\}$ surface as a function of the slab thickness. The number n indicates the number of layers in the slab. $\Delta d_{ij} = 100(d_{ij} - d_0)/d_0$, where d_{ij} is the spacing between the atomic layer i and j . d_0 is the interlayer spacing of bulk-truncated surface, $d_0 = 1.805$ Å. The + and - signs represent inward and outward relaxations of the interlayer spacing, respectively. Work function of the bare slab, $\Phi^{\text{Pd}(100)}$, is also listed below.

Layer or Method	Δd_{12} (%)	Δd_{23} (%)
5	-1.1	+0.57
7	-1.1	+0.42
9	-1.1	+0.48
DFT+USPP ^a	-1.0	+0.1
LEED ^b	+4.6	+0.3
LEED ^c	0	/
$\Phi^{\text{Pd}(100)}$	5.12 (this work), ^d 5.14, ^a 5.22 ^e	

^aReference 39.

^bReference 40.

^cReference 41.

^dThis work.

^eReference 45.

TABLE III. Energetic and structural parameters for H₂O at stable (atop) and metastable (bridge and hollow) sites of Pd {100}. E_{ads} is the adsorption energy (eV), which is defined as $E^{\text{ads}} = E^{\text{water/slab}} - E^{\text{slab}} - E^{\text{water}}$. $\Delta\Phi$ stands for work function change upon adsorptions, which is defined as $\Delta\Phi = \Phi^{\text{water/slab}} - \Phi^{\text{slab}}$. d_{OH} is the bond length. θ is the HOH angle. $d_{\text{O-Pd}}$ is the distance of oxygen atom to the metal surface. Δ_{xy} is the displacement of the oxygen atom from its precise original place. All the distance are in Å unit.

Site	d_{OH} (Å)	θ (deg)	$d_{\text{O-Pd}}$ (Å)	Δ_{xy} (Å)	E_{ads} (eV)	$\Delta\Phi$ (eV)
α -atop	0.98	104.6	2.49	0.10	-0.28	-0.77
β -atop	0.98	104.5	2.49	0.15	-0.28	-0.69
β -bridge	0.98	103.5	2.72	0.18	-0.16	-0.09
γ -bridge	0.98	107.6	2.31	0	-0.09	-2.12
α -hollow	0.98	103.7	2.86	0.31	-0.15	+0.13
β -hollow	0.98	103.0	2.61	0.80	-0.17	+0.18
γ -hollow	0.98	105.5	2.90	0	-0.02	-1.98

an insignificant expansion for the second Pd interlayer spacing (d_{23}) was observed. Though this observation is in agreement with previous density functional theory (DFT) results,³⁹ it is, however, inconsistent with LEED data.^{40,41} Similar discrepancy was also reported for the Pd {111} surface.^{42,43} The outward relaxation in the LEED data could be due to the presence of some residual hydrogen, as indicated by Jung and Kang.⁴⁴ Therefore, the relaxation pattern presented here is representative of a true surface relaxation for clean Pd {100}. The calculated work function of the clean Pd {100} is in good agreement with DFT³⁹ and experimental results.⁴⁵

B. Adsorption structures

To obtain a comprehensive search, water was initially placed on the precise high-symmetry sites (atop, bridge, and hollow) with various orientations with respect to the substrate. Compared with its state in the gas phase, the bond length of H₂O was enlarged by 0.1 Å due to the adsorption over various sites, while no prominent change on the bond angle was found (Table III).

The near atop region with a radius of 0.6 Å was carefully explored to obtain the globally stable configuration. Our results show that the water monomer adsorbs weakly but preferentially at atop site with an adsorption energy of -0.28 eV (Table III). This adsorption site is in agreement with the EELS results of H₂O on Pd {100} at about 10 K.⁸ We notice

that the adsorption energy is similar to that of H₂O adsorption on Pd (111): -0.33 eV (Ref. 26) and -0.30 eV,²⁷ indicating that the nature of H₂O-Pd interaction is localized and independent of whether the surfaces have a hexagonal lattice or square symmetry. Moreover, two different water orientations (α and β) were identified as the most stable structures [Figs. 1(a) and 1(b)], interestingly, with the same adsorption energy (-0.28 eV). The molecular plane is nearly at right angle to the surface normal, suggesting a flat-lying configuration of the adsorption. The oxygen atom is slightly displaced from the precise on-top sites (0.15 Å for α -atop, 0.10 Å for β -atop). The two molecular orientations obtained (α and β), with molecular axis along $\langle 011 \rangle$ and $\langle 001 \rangle$ directions, respectively, possess the highest symmetry match with the substrate of square lattice. The obtained barrier, for switching orientations between α and β by rotation, was found to be very low (0.02 eV), indicating that the potential energy surface of the adsorption is fairly flat within the atop site. This is in agreement with our previous results for water on Al {100},⁴⁶ as well as those from other investigations²⁷ suggesting that vibrational reorientations are active for a confined monomer within the adsorption well, even at much lowered temperatures.

Besides the stable on-top adsorption with the flat-lying configurations, metastable structures (local minimum energy) of water adsorption over the bridge and hollow sites were found, and the structural and energetic data are also listed in Table III. The hydrogen-up configuration over the bridge and

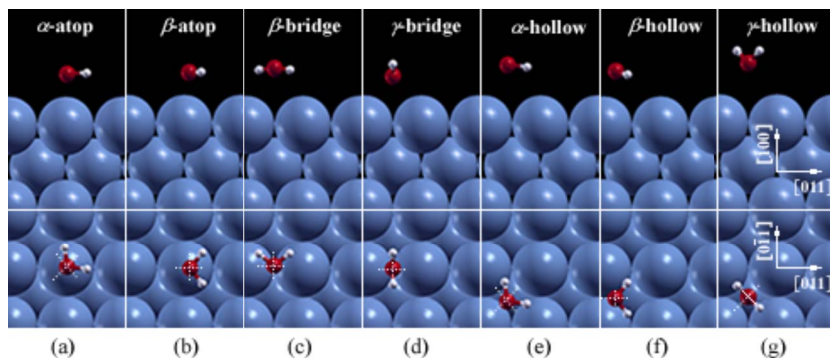


FIG. 1. (Color online) Top view (lower panels) and side view (upper panels) of the optimized structures of adsorbed H₂O on Pd {100} surface: (a) α -atop, (b) β -atop, (c) β -bridge, (d) γ -bridge, (e) α -hollow, (f) β -hollow, and (g) γ -hollow. The plane directions for each panel were indicated in the rightmost panels. The adsorption energies as well as structural parameters for each configuration are listed in Table III.

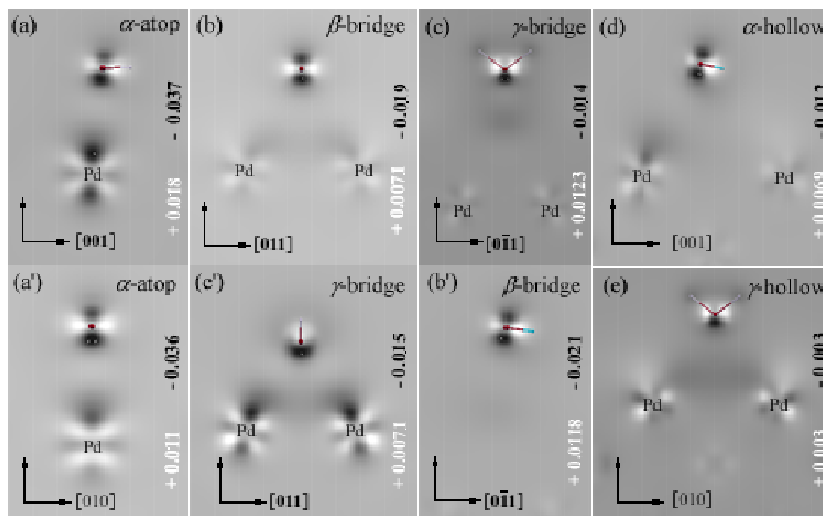


FIG. 2. (Color online) The two-dimensional (2D) contour plots of electron density difference for water adsorption on Pd {100}. (a) α -atop, (b) β -bridge, (c) γ -bridge, (d) α -hollow, (e) β -hollow, and (f) γ -hollow adsorption. Cross sections are shown in directions passing through the oxygen atom as indicated in Fig. 1. The plots were obtained by subtracting from the adsorption system the densities of a clean Pd slab and a H₂O molecule: $\Delta n(\mathbf{r}) = n^{\text{water/metal}}(\mathbf{r}) - n^{\text{metal}}(\mathbf{r}) - n^{\text{water}}(\mathbf{r})$. The 2D contour maps were drawn in linear scale from $[\Delta n(\mathbf{r})_{\min}]$ to $[\Delta n(\mathbf{r})_{\max}]$, represented by the color gradient. Negative $\Delta n(\mathbf{r})$ indicates loss of electron density upon binding, while a positive one corresponds to electron density accumulation. The values of $\Delta n(\mathbf{r})_{\min}$ and $\Delta n(\mathbf{r})_{\max}$ are also shown on the right side of each map; the white balls mark the position of Pd atoms.

hollow sites was obtained and denoted as γ -bridge [Fig. 1(d)] and γ -hollow [Fig. 1(g)], respectively. It is interesting to note that the configurations possess high symmetrical match for the H₂O-Pd interactions; however, the adsorption was very unstable due to the low adsorption energy (-0.09 eV for γ -bridge, -0.02 eV for γ -hollow). Other metastable configurations with various displacements from the precise bridge and hollow sites were identified as the β -bridge [Fig. 1(c)], α -hollow [Fig. 1(e)], and β -hollow [Fig. 1(f)].

For identified structures of α -hollow and β -hollow, the displacements from the precise hollow sites are so pronounced that the oxygen is closer to the atop and bridge sites. Nevertheless, the two structures exhibit clear characteristics of negative horizontal angles which were not reported by previous studies, and therefore, are considered distinct from Figs. 1(a) and 1(c), respectively. In considering the relationship between the vertical distance of the oxygen from a substrate and the adsorption energy thereof, Meng *et al.*²⁷ claimed that a strong adsorption corresponds to a shorter oxygen-metal bond. Our results, however, show that such is not the case for water adsorption on Pd {100}, where the shortest distance for γ -bridge adsorption exhibited a much weaker adsorption energy [Fig. 1(d)]. This, in fact, demonstrates the importance of molecular degrees of freedom in understanding water-Pd interactions, as is the case with molecular symmetries in surface diffusion.⁴⁶ The positive correlation between the two quantities, which is applicable for atomic adsorptions, is invalid for water-metal interaction in general. Caution must be taken when estimating and comparing adsorption energy from water-metal distances, as well as other molecules' adsorption on metals. This is due essentially to different effects of the Pauli exclusion principle for up-

right water over bridge sites. In addition, we performed calculations of work function change ($\Delta\Phi$) upon the water adsorptions, and the results are listed in Table III. $\Delta\Phi = -0.77$ or -0.69 eV for the on-top adsorption is close to experimental values,^{19,20} showing the validity of the current results. The greatest variations of work function were found for the upright water adsorption over the bridge and hollow sites. However, the order of $\Delta\Phi$ is obviously not inline with that of the adsorption energy. Our finding, together with results of water layers on Cu(110),⁴⁷ suggests that identification of stable adsorptions on the basis that a large work function change on adsorption correspond to favored adsorptions may not be correct.

C. Electronic structures

To understand the obtained geometrical picture of water adsorption, we calculated the electron density differences to characterize electron redistribution and possible bonding orbitals in the adsorption of water monomer on the various high-symmetry sites. Considering the α -atop adsorption, water-palladium interactions accumulate electrons in a region circling around the oxygen. Electronic polarization in this region showed higher accumulation of electrons on sides with H atoms present. This is illustrated in the cross-sectional view cutting along the molecular axis [Fig. 2(a)]. Electrons were found to be removed from a $1b_1$ -like orbital that is intercrossed and orthogonal to the accumulation region. A more severe depletion of electron can be observed within the down leaf of this orbital toward the surface bonding atom, suggesting a clear polarization of the state upon adsorption. The electron rearrangement of the bonding Pd

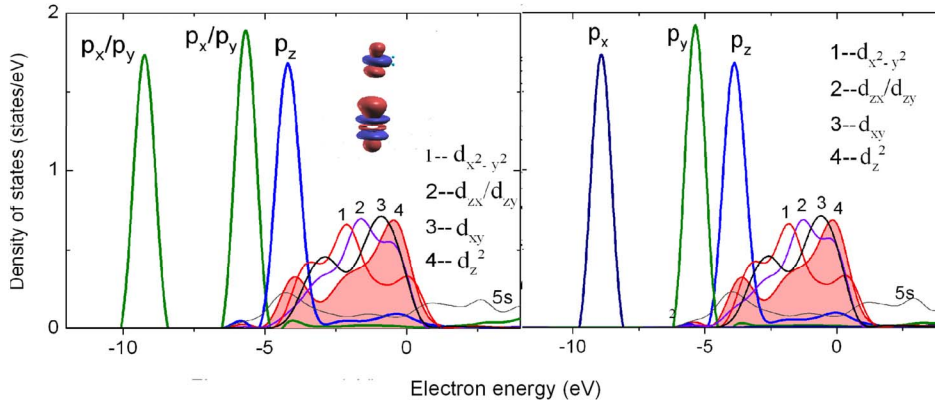


FIG. 3. (Color online) Density of states of (a) α -top and (b) β -top adsorptions. The 3D isosurface value of the electron density difference (inset) is set at $\pm 0.005 e/\text{\AA}^3$.

beneath the oxygen exhibits pronounced characteristics of the d_z^2 and diagonal states (d_{zx} and d_{zy}) [Figs. 2(a) and 2(a')]. Electrons rearranged and accumulated in the d_{zx} - and d_{zy} -like orbitals, while the d_z^2 -like state, which is responsible for the electron depletion, stretched toward the $1b_1$ -like orbital of the water. However, the two depletion regions ($1b_1$ -like and d_z^2 -like) are not directly overlapped, and interestingly, a region of slight electron accumulation sandwiched between them is discernible. We attribute this feature to the electron backdonation and electron transfer from d_z^2 to $5s$ state (see PDOS below), which are fundamentally different from the view for water on Ru {1000} reported by Michaelides *et al.*²⁶ that $1b_1$ - d_z^2 transferred electrons into the diagonal states (d_{zx} and d_{zy}). We found that electron redistribution for the beta orientation is in line with that of the alpha, indicating that $1b_1$ - d_z^2 interaction plays a key role in water-palladium interaction at the on-top sites.

A clear feature of the over-bridge adsorption is the distorted orbitals of electron accumulation and depletion in which d_z^2 incline toward each other and slightly get overlapped, stretching out toward the oxygen over the bridge site [Fig. 2(b)]. This redistribution pattern can also be found in the γ -hollow adsorption [Fig. 2(e)], and is more clearly represented in the upright configuration [Fig. 2(c')]. Moreover, a special electron rearrangement with the upright water [Fig. 2(c)] can be observed where electron depletion and accumulation are localized in the region just below the oxygen and in the regions near the oxygen along the OH bonds, respectively. The hollow adsorption [Fig. 2(e)] exhibits similar distribution as well. These observations suggest that hybridization of d_z^2 - p_z or d_z^2 - p_y accounts for the adsorption at bridge and hollow sites.

To further understand the nature of water adsorptions and how exactly the orbitals are involved in the H_2O -Pd interactions, we calculated the PDOS, an important method for characterizing bonding orbitals of the various adsorption sites. Each PDOS was projected onto the p states (p_x , p_y , and p_z) of the oxygen, the $4d$ states (d_z^2 , d_{zx} , d_{zy} , $d_{x^2-y^2}$, and d_{xy}), and the $5s$ state of the Pd beneath the adsorbed water. The d components that are not involved in the adsorption are also shown in the inset figure. Three-dimensional (3D) electron density difference, which is obtained by subtracting from the adsorption system the densities of a clean Pd slab and a H_2O

molecule: $\Delta n(\mathbf{r}) = n^{\text{water/metal}}(\mathbf{r}) - n^{\text{metal}}(\mathbf{r}) - n^{\text{water}}(\mathbf{r})$, is also shown in each figure. Negative (red) $\Delta n(\mathbf{r})$ indicates loss of electron density upon binding, while a positive (blue) one corresponds to electron density accumulation.

From the PDOS of α -top adsorption [Fig. 3(a)], we found that an adsorption-induced energy splitting of the d_z^2 state exhibiting a triplet feature, rather than other components of Pd $4d$ states (inset figure), plays a key role in the water-palladium interaction. With increasing energy, each of the subpeaks of d_z^2 in increasing intensity resonates more or less with molecular orbitals of the water, resulting in a triplet resonance of H_2O -Pd bonding. The hybridization degree, however, does not follow the sequence of the intensity of the subpeaks, and the strongest resonance takes place at the intermediate peak of d_z^2 . This resonance at the main peak of p_z , which involves combinations of the states of p_z , d_z^2 , p_x/p_y , and $5s$, constitutes a major hybridization of H_2O -Pd interaction. This result is substantiated by the 3D electron density difference shown as in the inset of the figure. For all the involved states, possible overlaps, in the order of decreasing interaction efficiency, include p_z - d_z^2 , p_z - $5s$, p_x/p_y - d_z^2 , and p_x/p_y - $5s$.

These results provide evidence that the p_z - d_z^2 interaction is involved in the on-top adsorption and also that the role of $5s$ in the bonding is indispensable. The weak resonance (first resonance) at the p_x/p_y peak of higher energy is a combination of d_z^2 , p_x/p_y , and p_z (namely, the interaction of $3a_1$ - d_z^2). The third resonance at the energy of the main peak of d_z^2 is a combination of p_z and d_z^2 , which is stronger than the first resonance, but is still far weaker than the second one. Interestingly, the roles of d_z^2 in the second and third resonances are distinct, whereby d_z^2 serves as an acceptorlike orbital in the former and as a donorlike one in the latter.

According to configuration principle, electron occupation of $5s$ at ground state has priority over that of $4d$ for the Pd electronic configuration $[\text{Kr}] 4d^{10}5s^0$. From the PDOS analysis, we found that all the d components were not fully occupied for the adsorption over the various high-symmetry sites, which is a consequence of the partial electron transference into $5s$ state. We found that $5s$ is partially occupied, and that the state below the Fermi level serves as the bonding state, which shows a clear adsorption-induced resonance at the energy of the p_z main peak, while the state above the Fermi

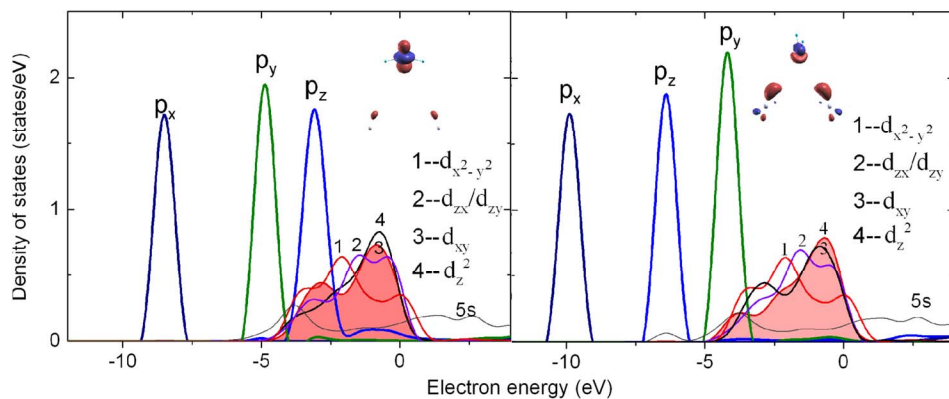


FIG. 4. (Color online) Density of states of the (a) β -bridge and (b) γ -bridge adsorptions. The 3D isosurface value of the electron density difference (inset) is set at 0.005 and $\pm 0.004 e/\text{\AA}^3$, respectively.

level contributes to the antibonding state. It is noteworthy that bonding-antibonding splittings below the Fermi level are also observed here.

Compared with the beta adsorption [Fig. 3(b)], we found some consistent similarities of the PDOS between the two orientations of the on-top adsorptions, along with the following discrepancies. (a) Both p_x and p_y states exhibit doublet structures for the alpha orientation, but nearly singlet structures for the two orbitals were observed for the beta adsorption. (b) p_x and p_y are degenerate at the energies of the peaks for alpha adsorption, while it is not so for beta orientation. (c) Hybridization involving d_z^2 with both p_x and p_y states is presented in the second resonance for α -atop adsorption, whereas p_x state is absent for the beta orientation. These observations show that the electronic nature of the on-top adsorptions can be somewhat different, even though the same energetic and structural picture is obtained.

In the case of adsorption over bridge sites, as illustrated in Fig. 4(a) for the β -bridge structure, the adsorption-induced doublet and triplet structures for d_{xy} and d_{zx} states, respectively, are involved in the resonances of the water-palladium interaction. The resonance at the energy of the main peak of p_z , which comprises hybridization of p_z with d_{xy} or d_{zx} and a small amount of overlap of p_y with d_{xy} or d_{zx} , contributes the major energy of the adsorption. Another resonance near the Fermi level is also discernible, which is related to the hybridization of d_{xy} with p_z at the energy of the main peak of d_{xy} . For upright adsorption over the bridge site [Fig. 4(b)], only the p_y state is involved in the overlap with the subpeak of the

d_z^2 state, and the resonance is rather weak, resulting in low adsorption energy.

For the α -hollow site [Fig. 5(a)], the d_{xy} state is found to play a role in the hybridization involving an overlap with p_y and p_z . Similar electronic structure is found for the β -hollow configuration [Fig. 5(b)]. An additional state, d_{zy} , is observed. Moreover, the resonance of p_y and d_{xy} is stronger than that of any other configuration in our analysis. The weakest adsorption, upright water over the hollow site, exhibits no clear hybridizations between orbitals of the water and those of the substrate.

From optimized structures, we notice that the adsorbed water exhibits either a flat-lying configuration or an upright one. A common feature of the flat-lying adsorption, from electron density difference, is the interaction of $1b_1$ -like molecular orbital with the Pd d_z^2 state. $3a_1$ -like orbital is the preferred adsorption with the upright structure. We notice that this is a general rule for water adsorption on metals, as reported in the previous study. In the framework of the frontier-orbital theory, these orbital overlaps meet symmetry-match standards, and therefore, gain relatively stable adsorptions. This is confirmed by our 3D electron density difference as well as the results of electron density of states. Moreover, PDOS analyses reveal that the energy shifts of the orbital resonance at the energy of the main peak of the p_z state are more pronounced for the two on-top adsorptions, suggesting greater charge transference between the adsorbate and the substrate, and therefore, a stronger binding energy compared to that on other sites.

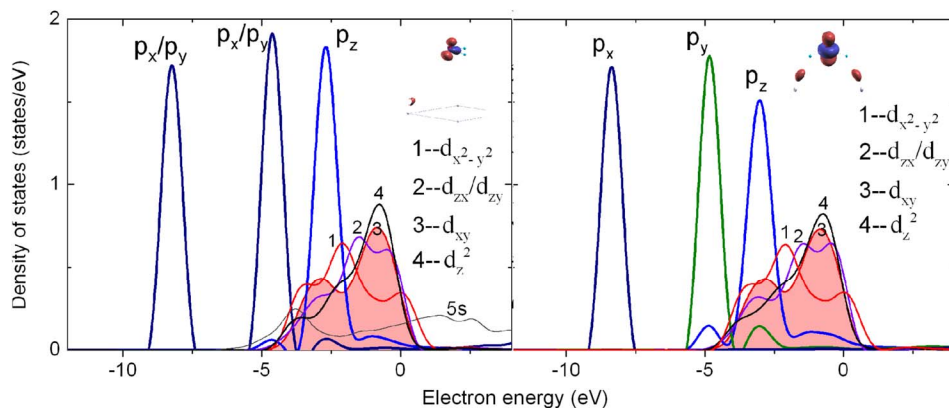


FIG. 5. (Color online) Density of states of the (a) α -hollow and (b) β -hollow adsorptions. The 3D isosurface value of the electron density difference (inset) is set at ± 0.004 , ± 0.004 , and $\pm 0.002 e/\text{\AA}^3$, respectively.

IV. CONCLUSIONS

Monomeric water adsorption on various sites of Pd {100} has been investigated within the framework of the density functional theory. We have presented a detailed picture of the electronic structure for the adsorptions by using work function analysis, charge density difference, and partial density of states. We have reported a counterintuitive relationship between the vertical distance of the oxygen (γ -bridge) from the substrate and the adsorption energy thereof. In addition to the well-recognized role of the d_z^2 orbital, some other d orbitals were found responsible for the adsorption nature of the water-metal interactions. We have shown that

Pd $5s$ state plays an indispensable role in water adsorptions including the favored on-top case, which has not been previously reported. Our results suggest that it is improper to treat the electronic nature of water-metal interactions as the simple regime of $1b_1-d_z^2$ or $3a_1-d_z^2$ hybridization.

ACKNOWLEDGMENTS

The authors are very grateful to all colleagues who assisted with useful discussions on this topic, particularly D. G. Lees and E. E. Oguzie. This work is partially supported by the National Science Foundation (NSF) under Contract No. 50671113.

*Authors to whom correspondence should be addressed.

[†]jibiaoli@imr.ac.cn

[‡]fhwang@imr.ac.cn

¹P. A. Thiel and T. E. Madey, *Surf. Sci. Rep.* **7**, 211 (1987).

²M. A. Henderson, *Surf. Sci. Rep.* **46**, 1 (2002).

³C. D. Taylor and M. Neurock, *Curr. Opin. Solid State Mater. Sci.* **9**, 49 (2005).

⁴C. Clay and A. Hodgson, *Curr. Opin. Solid State Mater. Sci.* **9**, 11 (2005).

⁵G. Pauer and A. Winkler, *J. Chem. Phys.* **120**, 3864 (2004).

⁶T. Mitsui, M. K. Rose, E. Fomin, D. F. Ogletree, and M. Salmeron, *Surf. Sci.* **511**, 259 (2002).

⁷J. P. McEvoy and G. W. Brudvtg, *Chem. Rev. (Washington, D.C.)* **106**, 4455 (2006).

⁸S. Anderson, C. Nyberg, and C. G. Tengstal, *Chem. Phys. Lett.* **104**, 305 (1984).

⁹C. Nyberg, C. G. Tengstal, P. Uvdal, and S. Anderson, *J. Electron Spectrosc. Relat. Phenom.* **38**, 299 (1986).

¹⁰C. Nyberg and C. G. Tengstal, *J. Chem. Phys.* **80**, 3463 (1984).

¹¹E. M. Stuve, S. W. Jorgensen, and R. J. Madix, *Surf. Sci.* **146**, 179 (1984).

¹²K. G. Lloyd, B. A. Banse, and J. C. Hemminger, *Phys. Rev. B* **33**, R2858 (1986).

¹³R. Brosseau, T. H. Ellis, and M. Morin, *J. Vac. Sci. Technol. A* **8**, 2454 (1990).

¹⁴R. Brosseau, M. R. Brustein, and T. H. Ellis, *Surf. Sci.* **280**, 23 (1993).

¹⁵R. Brosseau, T. H. Ellis, M. Morin, and H. Wang, *J. Electron Spectrosc. Relat. Phenom.* **54-55**, 659 (1990).

¹⁶Minsheng Xu, Ping Yang, Wei Yang, and Shijin Pang, *Vacuum* **43**, 1125 (1992).

¹⁷M. Wolf, S. Nettesheim, J. M. White, E. Hasselbrink, and G. Ertl, *J. Chem. Phys.* **92**, 1509 (1990).

¹⁸M. Wolf, S. Nettesheim, J. M. White, E. Hasselbrink, and G. Ertl, *J. Chem. Phys.* **94**, 4609 (1991).

¹⁹J. M. Heras, G. Estiú, and L. Viscido, *Appl. Surf. Sci.* **108**, 455 (1997).

²⁰Jian-Wei He and P. R. Norton, *Surf. Sci.* **238**, 95 (1990).

²¹T. Mitsui, M. K. Rose, E. Fomin, D. F. Ogletree, and M. Salmeron, *Science* **297**, 1850 (2002).

²²J. Cerda, A. Michaelides, M. L. Bocquet, P. J. Feibelman, T. Mitsui, M. Rose, E. Fomin, and M. Salmeron, *Phys. Rev. Lett.*

93, 116101 (2004).

²³H. Ogasawara, B. Brena, D. Nordlund, M. Nyberg, A. Pelmenchikov, L. G. M. Pettersson, and A. Nilsson, *Phys. Rev. Lett.* **89**, 276102 (2002).

²⁴G. S. Karlberg, *Phys. Rev. B* **74**, 153414 (2006).

²⁵A. Michaelides, A. Alavi, and D. A. King, *J. Am. Chem. Soc.* **125**, 2746 (2003).

²⁶A. Michaelides, V. A. Ranea, P. L. de Andres, and D. A. King, *Phys. Rev. Lett.* **90**, 216102 (2003).

²⁷S. Meng, E. G. Wang, and Shiwu Gao, *Phys. Rev. B* **69**, 195404 (2004).

²⁸V. A. Ranea, A. Michaelides, R. Ramírez, J. A. Vergés, P. L. de Andres, and D. A. King, *Phys. Rev. B* **69**, 205411 (2004).

²⁹D. Sebastiani and L. D. Site, *J. Chem. Theory Comput.* **1**, 78 (2005).

³⁰Sanwu Wang, Yanzhao Cao, and P. A. Rikvold, *Phys. Rev. B* **70**, 205410 (2004).

³¹A. Nilsson and L. G. M. Pettersson, *Surf. Sci. Rep.* **55**, 49 (2004).

³²S. Baroni, A. Dal Corso, S. de Gironcoli, P. Giannozzi, C. Cavazzoni, G. Ballabio, S. Scandolo, G. Chiarotti, P. Focher, A. Pasquarello, K. Laasonen, A. Trave, R. Car, N. Marzari, and A. Kokalj, QUANTUM ESPRESSO, opEn-Source Package for Research in Electronic Structure, Simulation, and Optimization, <http://www.quantumespresso.org>.

³³A. Kokalj, *Comput. Mater. Sci.* **28**, 155 (2003); code available from <http://www.xcrysden.org/>

³⁴David Vanderbilt, *Phys. Rev. B* **41**, R7892 (1990).

³⁵J. P. Perdew, J. A. Chevary, S. H. Vosko, K. A. Jackson, M. R. Pederson, D. J. Singh, and C. Fiolhais, *Phys. Rev. B* **46**, 6671 (1992).

³⁶J. P. Perdew, K. Burke, and M. Ernzerhof, *Phys. Rev. Lett.* **77**, 3865 (1996).

³⁷Hendrik J. Monkhorst and James D. Pack, *Phys. Rev. B* **13**, 5188 (1976).

³⁸David R. Lide, *Handbook of Chemistry and Physics* (CRC, Boca Raton, FL, 2004).

³⁹A. Eichler, J. Hafner, and G. Kresse, *J. Phys.: Condens. Matter* **8**, 7659 (1996).

⁴⁰J. Burchhardt, E. Lundgren, M. M. Nielsen, J. N. Andersen, and D. L. Adams, *Surf. Rev. Lett.* **3**, 1339 (1996).

⁴¹S. H. Kim, H. L. Meyerheim, J. Barthel, J. Kirschner, J. Seo, and J. S. Kim, *Phys. Rev. B* **71**, 205418 (2005).

- ⁴²T. E. Felter, E. C. Sowa, and M. A. VanHove, *Phys. Rev. B* **40**, 891 (1989).
- ⁴³M. A. Ohtani, M. A. van Hove, and G. A. Somorjai, *Surf. Sci.* **187**, 372 (1987).
- ⁴⁴S. C. Jung and M. H. Kang, *Phys. Rev. B* **72**, 205419 (2005).
- ⁴⁵F. Besenbacher, I. Stensgaard, and K. Mortensen, *Surf. Sci.* **191**, 288 (1987).
- ⁴⁶Jibiao Li, Y. Li, S. Zhu, and F. Wang, *Phys. Rev. B* **74**, 153415 (2006).
- ⁴⁷J. Ren and S. Meng, *J. Am. Chem. Soc.* **128**, 9282 (2006).